Multi-objectives Integrated Division-Summation Method for LCL-Type Three-Level Grid-Connected Inverter Considering Low- Frequency Common Mode Voltage

Jiang Liu, *Member IEEE*, Weizhang Song, Dong Ding, Zechi Chen,
Patrick Wheeler, *Fellow IEEE*, and Siya Sun

***Abstract*- The LCL-type three-level grid-connected inverter is extensively employed in photovoltaic (PV) power generation systems, which has multiple individually controlled objectives. To this end, an integrated Division-Summation (I-D-Σ) control strategy is proposed in this paper, which can consider grid-connected current tracking, neutral-point potential (NPP) balance control, resonance suppression and low-frequency common mode voltage (CMV), simultaneously. To compensate for the fact that the Dual-Division-Summation (D-D-Σ) method only considers grid-connected current and resonance suppression, a virtual zero potential point is added for NPP balance control. Additionally, a low-frequency CMV estimation method based on Fully Connect-Convolutional Neural Network (FC-CNN) is proposed, which perfectly avoids the unobservability of sensorless CMV. The I-D-Σ method can effectively reduce the low-frequency CMV, which is compensated by the low-frequency CMV. The effectiveness of the proposed strategy was verified through comparative experimental results.**

***Index Terms*—I-D-Σ control strategy, zero potential point, common mode voltage, estimation method**

I. INTRODUCTION

PV power generation technology, as one of the renewable energy generation technologies, is an important energy supply in response to the energy conversion process [1]. As an DC/AC conversion equipment, the performance improvement of PV grid-connected inverter is related to energy conversion efficiency and power quality [2]. The LCL-type three-level PV grid-connected inverter has been widely used due to its higher power generation efficiency and higher grid-connected current power quality. The LCL-type three-level PV grid-connected inverter has numerous control objectives that controlled separately, such as grid-connected current, NPP balance, resonance suppression, and CMV [3].

Taking a single LCL-type three-level grid-connected inverter as an example, grid-connected current control is the primary goal. Common grid-connected current control methods include Proportional Integral (PI) control [4], Quasi Proportional Resonance (QPR) control [5], repetitive control [6], deadbeat control [7], D-Σ digital control [8], et al. Among them, PI and QPR control require coordinate transformation, which get poor control effect under unbalanced grid. Repetitive control has poor dynamic performance. Deadbeat control and D-Σ digital control have high response speed and control accuracy, but are highly dependent on circuit parameters. In order to expand the application of D-Σ control in LCL-type grid-connected inverter, a D-D-Σ control method combined with parameter estimation algorithm is proposed in [9] to compensate for the sensitivity problem of the D-Σ control method. For LCL-type inverter, resonance effects make its control more complex. The common resonance suppression methods can be divided into passive and active damping methods [10]. The energy loss of passive damping methods leads to it not being separately suppressed for resonance. The mature active damping methods include state variable feedback method, impedance reshaping, et al. Generally, the grid-connected current control combined with resonance suppression can independently control the corresponding control objective to ensure the power quality of the AC-side of the grid-connected inverter. Even though the D-D-Σ strategy can simultaneously control the grid-connected current and resonance, it uses the injection NPP balance method. The NPP fluctuation and low-frequency CMV are not considered in the derivation process of the D-D-Σ strategy. The NPP balancing methods can be divided into additional balancing circuit [11], modulation-based method [12] and zero-sequence component injection method [13]. However, the NPP balance method based on modulation strategy is more complex, which has huge amount of calculation. The zero-sequence component injection method requires high sampling accuracy for grid-connected current. In addition, the CMV will appear in the topology without connection between the DC-side and the neutral-point of the grid. Generally, the CMV includes the high-frequency CMV with switching frequency times and the low-frequency CMV with zero-sequence component injection, which is three times the fundamental frequency [14]. There are many methods to optimize modulation strategies for suppressing high-frequency CMV or considering both high-frequency CMV and NPP balance [15][16]. However, low-frequency CMV is also a concern in CMV-related problems such as challenges with filter design [14].

Although the above four objectives have achieved good results when controlled separately or partially, there are few control algorithms that can be applied to multiple control objectives. Model predictive control (MPC) is a global control method that can simultaneously consider the multiple objectives, which is also widely used in three-level grid-connected inverter [17][18]. There is no reported integrated

control method that can fully consider the four control objectives described in this paper. Even with MPC, due to the lack of sensors for CMV, optimization modulation strategies are still used to suppress high and low frequency CMV. The closed-loop or injection based low-frequency CMV suppression methods have not yet been developed.

In order to achieve multi-objectives integrated control of LCL-type three-level grid-connected inverter, the main research contributions in this paper are as follows.

(1) Based on D-D-Σ control method, an I-D-Σ control method which can realize multi-objectives integrated control is proposed in this paper. The proposed method can simultaneously consider the grid-connected current, NPP balance, resonance suppression and low-frequency CMV.

(2) During the derivation of I-D-Σ control method, a concept of virtual zero potential point is proposed to balance the fluctuation of NPP.

(3) A low frequency common mode voltage injection suppression method is proposed. A FC-CNN method is used to estimate the low-frequency CMV, which can avoid the unobservability of CMV.

This paper is organized as follows. In Section II, the specific derivation process of I-D-Σ control method is introduced in detail. The unobservability and estimation method of low-frequency CMV are proposed in Section III. Section IV demonstrates the effectiveness of the proposed method through experimental results.

II. Principle of I-D-Σ Control Strategy

Taking the LCL-type T-type three-level grid-connected inverter as an example, which is shown in Fig. 1, U_{dc} is the DC-side voltage. C_{a1} and C_{a2} are DC-side capacitances, and u_{Ca1} and u_{Ca2} represent their voltage values, respectively. L_{xi}, L_{xg} and C_x are components of LCL filters. i_{xi} and i_{xg} represent x-phase current of L_{xi} and L_{xg}, respectively. U_{PCCx} represents the x-phase grid voltage. Where, x= a, b, c.

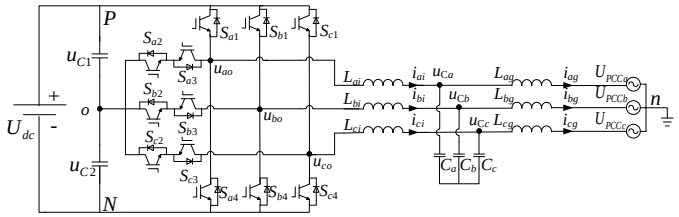

Fig. 1. Topology of LCL-type T-type three-level inverter.

According to Kirchhoff's Voltage Law, the mathematical model of the AC-side of the inverter can be expressed as:

$$L_{xi}\frac{di_{xi}}{dt}+L_{xg}\frac{di_{xg}}{dt}=u_{xo}+u_{on}-U_{PCCx} \tag{1}$$

Where, u_{xo} is the x-phase output voltage of the inverter to point o, and u_{on} is CMV between point o and point n.

Assuming a virtual zero potential point O of DC-side neutral point, Eq. (1) can be converted to:

$$L_{xi}\frac{di_{xi}}{dt}+L_{xg}\frac{di_{xg}}{dt}=u_{xO}+u_{Oo}+u_{on}-U_{PCCx} \tag{2}$$

Where, u_{xO} is the x-phase output voltage of the inverter to point O, which refers to the voltage under balanced NPP. u_{xO} is the voltage between point O and point o.

Based on the above definition, it can be obtained that:

$$u_{oo_1}=u_{C1}-u_{C2} \tag{3}$$

Within the positive and negative half cycle of the modulation wave, substituting Eq. (3) into Eq. (2) can obtain:

$$L_{xi}\frac{di_{xi}}{dt}+L_{xg}\frac{di_{xg}}{dt}=\begin{cases}\dfrac{U_{dc}}{2}-\left(u_{C1}-u_{C2}\right)+u_{on}-U_{PCCx} & t\in[T_s,T_s+t_{Pon})\\ -\left(u_{C1}-u_{C2}\right)+u_{on}-U_{PCCx} & t\in(T_s+t_{Pon},2T_s]\\ -\dfrac{U_{dc}}{2}-\left(u_{C1}-u_{C2}\right)+u_{on}-U_{PCCx} & t\in[T_s,T_s+t_{Non})\\ -\left(u_{C1}-u_{C2}\right)+u_{on}-U_{PCCx} & t\in(T_s+t_{Non},T_s+1]\end{cases} \tag{4}$$

Where, n represents the sampling time. t_{Pon} represents the action time of $+U_{dc}/2$. t_{Non} represents the action time of $-U_{dc}/2$.

When the modulation wave is in positive half cycle, the inverter output voltage includes two working states $+U_{dc}/2$ and 0. Thus, the duty ratios in positive half cycle corresponding to $+U_{dc}/2$ (P), 0 (O)and $-U_{dc}/2$ (N) can be set to:

$$\begin{cases}d_{xP}=d_x\\ d_{xO}=1-d_x\\ d_{xN}=0\end{cases} \tag{5}$$

Where, d_x is the duty cycle expression. x = a, b, c.

Thus, the duty ratios in negative half cycle can be set to:

$$\begin{cases}d_{xP}=0\\ d_{xO}=1+d_x\\ d_{xN}=-d_x\end{cases} \tag{6}$$

Division:

During positive half cycle $T_s/2$, the division of the inverter-side inductance current and grid-connected current in positive half cycle can be obtained as:

$$\begin{cases}2L_{xg}\Delta i_{xgP+}+2L_{xi}\Delta i_{xiP+}\\ =\left[U_{dc}/2-\left(u_{C1}-u_{C2}\right)+u_{on}-U_{PCCx}\right]d_{xP}T_s\\ 2L_{xg}\Delta i_{xgO+}+2L_{xi}\Delta i_{xiO+}\\ =\left[-\left(u_{C1}-u_{C2}\right)+u_{on}-U_{PCCx}\right]d_{xO}T_s\\ \Delta i_{xgN+}=\Delta i_{xiN+}=0\end{cases} \tag{7}$$

Where, Δi_{xyz+} represents current variation in positive half cycle corresponding to working state z of phase x on y-side inductance under positive half cycle. x = a, b, c. y = i (inverter), g (grid). z = P, O, N.

During negative half cycle $T_s/2$, the division can be obtained as:

$$\begin{cases}\Delta i_{xgP-}=\Delta i_{xiP-}=0\\ 2L_{xg}\Delta i_{xgP-}+2L_{xi}\Delta i_{xiP-}\\ =\left[-\left(u_{C1}-u_{C2}\right)+u_{on}-U_{PCCx}\right]d_{xO}T_s\\ 2L_{xg}\Delta i_{xgO-}+2L_{xi}\Delta i_{xiO-}\\ =\left[-U_{dc}/2-\left(u_{C1}-u_{C2}\right)+u_{on}-U_{PCCx}\right]d_{xN}T_s\end{cases} \tag{8}$$

Where, Δi_{xyz-} represents current variation in negative half cycle corresponding to Δi_{xyz+}.

Summation:

Summing the current variations in equations (7) and (8), and substituting the duty cycle set in equations (5) and (6), the AC-side mathematical expression in a complete T_s can be obtained as follows:

$$L_{xg}\Delta i_{xg}+L_{xi}\Delta i_{xi}=\frac{U_{dc}}{2}d_xT_s-U_{PCCx}T_s-\left(u_{C1}-u_{C2}\right)T_s+u_{on}T_s \quad (9)$$

Where, Δi_{xy} is current variation of x-phase y-side inductor. y = i (inverter), g (grid).

Rewriting Eq. (9) to obtain the modulation wave expression as follows:

$$d_x=\frac{2L_{xg}\Delta i_{xg}}{U_{dc}T_s}+\frac{2L_{xi}\Delta i_{xi}}{U_{dc}T_s}+\frac{2\left(u_{C1}-u_{C2}\right)}{U_{dc}}-\frac{2u_{on}}{U_{dc}}+\frac{2U_{PCCx}}{U_{dc}} \quad (10)$$

The current variations can be obtained by subtracting the sampling value $i_x(n)$ at nth switching period from the current reference $I_{xref}(n+1)$ at the $(n+1)$th switching period, which is to achieve grid-connected current tracking. Eq. (11) represents the modulation wave expression under I-D-Σ control strategy:

$$\begin{aligned}d_x(n+1)=&\frac{2L_{xi}\left[I_{xgref}(n+1)-i_{xi}(n)\right]}{U_{dc}T_s}\\&+\frac{2L_{xg}\left[I_{xgref}(n+1)-i_{xg}(n)\right]}{U_{dc}T_s}\\&+\frac{2\left[u_{C1}(n)-u_{C2}(n)\right]}{U_{dc}}\\&-\frac{2u_{on}(n)}{U_{dc}}\\&+\frac{2U_{PCCx}}{U_{dc}}\end{aligned} \quad (11)$$

The resonance suppression effect is achieved by minimizing the current of the filtering capacitor [19]. Compared with the results in Ref. [9], the I-D-Σ control strategy proposed in this paper additionally considers NPP balance control and CMV. In Eq. (11), except for the CMV, all other variables can be obtained through sensors. In order to truly achieve integrated control of grid-connected inverter, it is necessary to estimate the low-frequency CMV.

III. Estimation Method of Low-Frequency CMV

A. Unobservable of CMV

Due to the lack of sensors for CMV, using the estimation method of unknown parameters, this paper tries to use the observer method [20]. Under I-D-Σ control strategy, the currents of L_{xi} and L_{xg} are considered to be consistent because the currents can be tracked accurately. The state equation of Eq. (1) can reasonably equate the LCL filter to an L filter. In general, if CMV is regarded as a disturbance, the state space equation can be obtained as Eq. (12) according to Eq. (1).

$$\frac{d}{dt}\begin{bmatrix}i_x\\u_{on}\end{bmatrix}=\begin{bmatrix}-\frac{R_x}{L_x}&\frac{1}{L_x}\\0&0\end{bmatrix}\begin{bmatrix}i_x\\u_{on}\end{bmatrix}+\begin{bmatrix}\frac{1}{L_x}\\0\end{bmatrix}\left[u_{xo}-U_{PCCx}\right] \quad (12)$$

Where, R is the equivalent resistance of filter inductance. u_{no} is treated as a slow-varying disturbance. Therefore, it can be considered that $du_{no}/dt = 0$ [21].

By discretizing (12), the state-space equation in the discrete time domain can be obtained as Eq. (13).

$$\begin{aligned}\begin{bmatrix}i_x(k+1)-i_x(k)\\u_{on}(k+1)-u_{on}(k)\end{bmatrix}=&\begin{bmatrix}-\frac{T_sR_x}{L_x}&\frac{T_s}{L_x}\\0&0\end{bmatrix}\begin{bmatrix}i_x(k)\\u_{no}(k)\end{bmatrix}\\&+\begin{bmatrix}\frac{T_s}{L_x}\\0\end{bmatrix}\left[u_{xo}(k)-e_x(k)\right]\end{aligned} \quad (13)$$

Eq. (13) can be rewritten as:

$$\begin{cases}\underbrace{\begin{bmatrix}i_x(k+1)\\u_{no}(k+1)\end{bmatrix}}_{\underline{\mathbf{x}}_{k+1}}=\underbrace{\begin{bmatrix}1-\frac{T_sR}{L_x}&\frac{T_s}{L_x}\\0&1\end{bmatrix}}_{\mathbf{A}_k}\underbrace{\begin{bmatrix}i_x(k)\\u_{no}(k)\end{bmatrix}}_{\underline{\mathbf{x}}_k}+\underbrace{\begin{bmatrix}\frac{T_s}{L_x}\\0\end{bmatrix}}_{\mathbf{B}_k}\underbrace{\left[u_{xo}(k)-e_x(k)\right]}_{\underline{\mathbf{u}}_k}\\\underbrace{\left[i_x(k)\right]}_{\underline{\mathbf{y}}_k}=\underbrace{\begin{bmatrix}1&0\end{bmatrix}}_{\mathbf{C}_k}\underbrace{\begin{bmatrix}i_x(k)\\u_{no}(k)\end{bmatrix}}_{\underline{\mathbf{x}}_k}\end{cases} \quad (14)$$

The observability matrix of Eq. (14) can be expressed as:

$$\mathbf{W}_O=\begin{bmatrix}\mathbf{C}_k\\\mathbf{C}_k\mathbf{A}_k\end{bmatrix}=\begin{bmatrix}1&0\\1-\frac{T_sR}{L_x}&\frac{T_s}{L_x}\end{bmatrix} \quad (15)$$

The rank of $\mathbf{W}_O$ can be obtained as 1. Therefore, Eq. (14) is unobservable. Meanwhile, Eq. (12) assumes that CMV is a slow-varying disturbance. In fact, CMV is a rapid-varying disturbance with low-frequency components and switching frequency components. Therefore, it further explains the unobservable of CMV.

B. Low-frequency CMV estimation method based on FC-CNN

The CMV of grid-connected inverter includes the low-frequency component caused by zero-sequence component injection and the high-frequency component caused by modulation strategy. Many references have proposed optimized modulation methods for high-frequency CMV suppression. This paper only considers the low-frequency CMV caused by zero-sequence component injection.

Recently, artificial intelligence (AI) based algorithms have been widely used in the fields of condition monitoring [22][23], fault diagnosis [24][25], intelligent optimization [26][27]. Among them, deep learning algorithms can mine data characteristics through a large number of training data, which has good applications in nonlinear modeling [28][29], load forecasting [30]. In this paper, the Fully Connected-Convolutional Neural Network (FC-CNN) is introduced to model and predict the low-frequency CMV [31].

As shown in Fig. 2, the constructed FC-CNN consists of input layer, one-dimensional convolution layer, adaptive average pooling layer, FC layer, and output layer. The hidden layer is composed of one-dimensional convolution layer, adaptive average pooling layer, and FC layer. One-dimensional convolution layer is used to extract features from the input vector $\mathbf{U}_{in}=[u_{xo},\ i_{xi},\ i_{xg},\ U_{PCCx}]^T$. Adaptive average pooling layer is used to reduce the dimensionality of feature extraction in convolutional layers while preserving key information in deep features. Multiple FC layers are used to calculate and characterize the mapping function between convolutional layer features and low-frequency CMV.

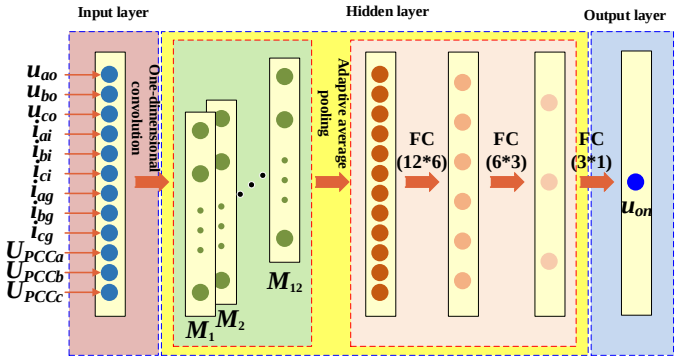

Fig. 2. Structure of the proposed FC-CNN used for low-frequency CMV estimation.

In Fig. 2, the input dimension is 12, which is the number of neurons in the input layer. In the hidden layer, $\boldsymbol{M}_1$, $\boldsymbol{M}_2$, … , $\boldsymbol{M}_{12}$ are one-dimensional convolution outputs of 12 channels. Then, three FC layers are used to find the mapping relationship between the output and features. ReLU activation function is used to connect each FC layer [32]. The output is low-frequency CMV with an output dimension of 1. The entire neural network training uses root mean square error as the loss function [33].

In actual grid-connected inverter systems, there are no sensors for the inverter output voltage, which is also a high-frequency signal. Therefore, a high-speed data acquisition system includes a LTC2290 chip (12-bit and 10MHz, from ADI company) and FPGA chip (ZYNQ7020 from Xilinx company) is designed to sample the data of u_{xo}, i_{xi}, i_{xg}, U_{PCCx}, and u_{on}. The collected data are processed by MATLAB software.

Selecting data from 10 power frequency cycles as training data, with a sampling frequency of 2.5MHz and an inverter switching frequency of 10kHz for the acquisition system. Firstly, the collected data are preprocess by taking the average of every 50 sampling points. The data within 10 power frequency cycles is 10000 sampling points. Secondly, low-pass filtering is applied to the processed output voltage and low-frequency CMV to retain the fundamental and triple fundamental frequency components. Finally, FC-CNN was used for offline training and validation, with validation data of 2 power frequency cycles. The training data can be represented as:

$$\left\{\left(\mathbf{U}_{in}^{1},u_{no}^{1}\right),\left(\mathbf{U}_{in}^{2},u_{no}^{2}\right),\ldots,\left(\mathbf{U}_{in}^{m},u_{on}^{m}\right)\right\} \tag{16}$$

Where, m is number of training data, m=10000.

Inputting the processed input vector and output variable data to FC-CNN to establish a mapping relationship. Assuming N and M are the number of neurons in the input layer and hidden layer, respectively. For the first hidden layer, the output $\mathbf{F}_1^k$ corresponding to the input vector $\mathbf{U}_{in}^k$ can be expressed as:

$$\mathbf{F}_1^k = f_h\left(\mathbf{W}_1\mathbf{U}_{in}^k+\mathbf{b}_1\right) \tag{17}$$

Where, $\mathbf{W}_1$ and $\mathbf{b}_1$ are weight parameters and bias parameters of first hidden layer, respectively. f_h is the activation function of the hidden layer.

The outputs $\mathbf{F}_2^k$ and $\mathbf{F}_3^k$ corresponding to the second hidden layer and the third hidden layer are obtained in the same way.

$$\begin{cases}\mathbf{F}_2^k = f_h\left(\mathbf{W}_2\mathbf{F}_1^k+\mathbf{b}_2\right)\\ \mathbf{F}_3^k = f_h\left(\mathbf{W}_3\mathbf{F}_2^k+\mathbf{b}_3\right)\end{cases} \tag{18}$$

Where, $\mathbf{W}_2$ and $\mathbf{b}_2$ are weight parameters and bias parameters of second hidden layer, respectively. $\mathbf{W}_3$ and $\mathbf{b}_3$ are weight parameters and bias parameters of third hidden layer, respectively.

Therefore, the output o^k of the entire hidden layer can be expressed as:

$$o^k = f_o\left(\mathbf{W}_4F_3^k+\mathbf{b}_4\right) \tag{19}$$

Where, f_o is the activation function of the output layer, and Sigmoid function is selected.

The goal of FC-CNN training is to minimize the difference between network output o^k and u_{on}^k. Therefore, the average loss function can be expressed as:

$$Loss(o)=\frac{1}{m}\sum_{k=1}^{m}l\left(u_{on}^k,o^k\right) \tag{20}$$

Where, l is root mean square loss function.

IV. Experimental Results

In order to verify the correctness of the proposed I-D-Σ control method, the hardware platform of T-type three-level inverter based on STM32F407+EPM240T100C5N control chips shown in Fig. 3 is built. The designed system transmits data to the upper computer through a sensor system. The upper computer uses FC-CNN to estimate low-frequency CMV, and then transmits it to ARM to implement I-D-Σ method. CPLD chip is used to process drive signals and incorporate dead zone and protection functions. The hardware parameters are shown in Table I. The control effects of grid-connected current, resonance, NPP balance and low-frequency CMV are verified, respectively.

TABLE I
EXPERIMENTAL PARAMETERS

Parameter	Value
DC-link voltage	200V
Grid voltage(pk-pk)	140V
Grid-connected current	10A
Inverter-side inductor L_{xi}	3.8mH
Grid-side inductor L_{xg}	1.1mH

Filter capacitor C_f	20μF
Fundamental frequency	50Hz
Switching frequency	10kHz

Sampling frequency	10kHz

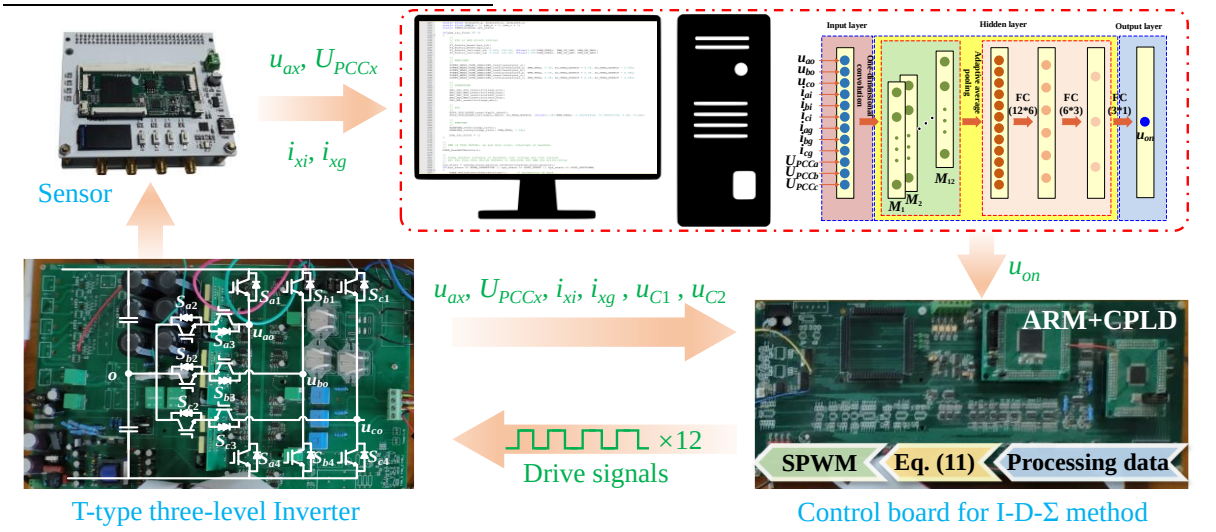

Fig.3 Experimental platform of a T-type three-level inverter with LCL filter.

Testing the experimental platform using the hardware parameters shown in Table I, and comparing the NPP balance control effect between the proposed I-D-Σ method and the D-D-Σ method with zero-sequence injection. The experiment results also compare the effects before and after the modulation wave with low-frequency CMV injection. Set two parameters as:

$$\begin{cases} K_{p1} = 2L_{xi} / (U_{dc} T_s) \\ K_{p2} = 2L_{xg} / (U_{dc} T_s) \end{cases} \tag{21}$$

A. Verification of grid-connected current tracking effect

Fig. 4 shows the dynamic waveforms of grid-connected currents under different grid-connected current control parameter K_{p2}. When the current reference value is 10A, according to the control parameter rules derived in this paper, it can stabilize the grid-connected currents at 10A. However, when the value of K_{p2} is reduced, it can be observed that after a brief fluctuation, the actual value of the grid-connected currents is less than 10A. Restoring the K_{p2} value can restore accurate tracking effect of grid-connected currents.

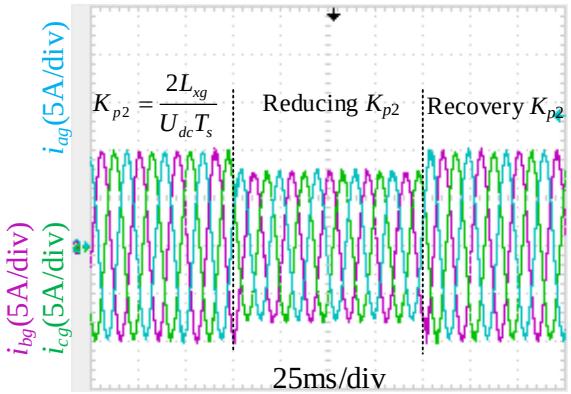

(a)

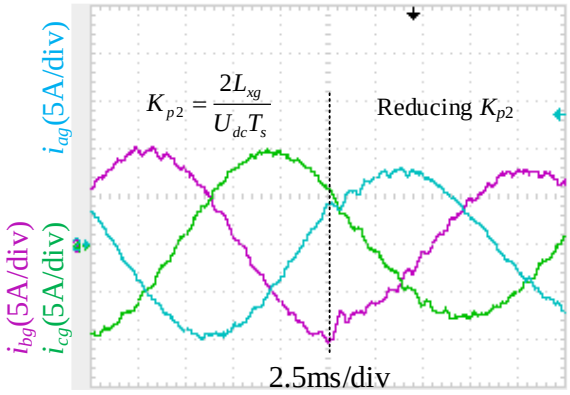

(b)

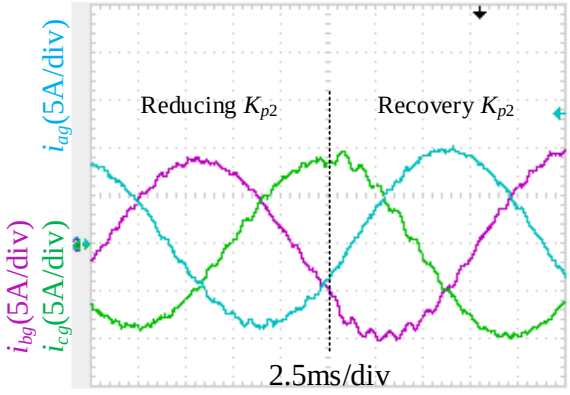

(c)

Fig.4 Grid-connected currents control effect of different K_{p2}. (a) Overall dynamic waveform. (b) Reducing K_{p2}. (c) Increasing K_{p2}.

B. Verification of resonance suppression effect

Fig. 5 shows the dynamic waveforms of grid-connected

currents under different resonance suppression parameter K_{p1}. The K_{p1} can make the grid-connected currents operate stably. However, reducing K_{p1} will trigger resonance, and harmonics appear in the grid-connected currents, as shown in Fig. 5 (b). Restoring the setting resonance suppression parameter K_{p1} can eliminate the resonance effect of grid-connected currents.

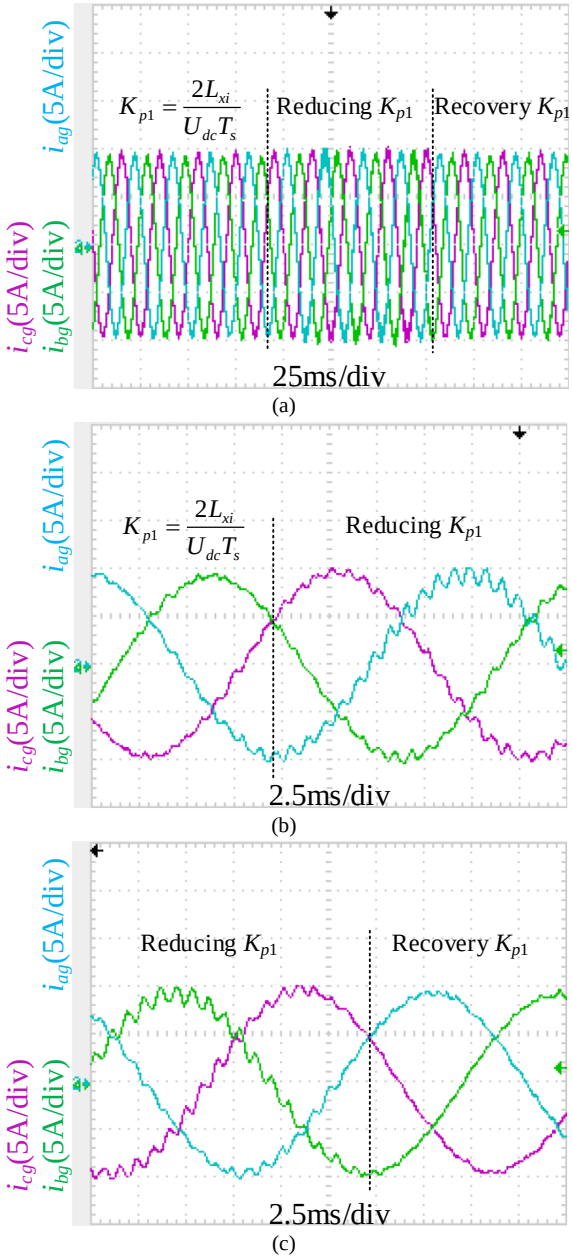

Fig.5 Resonance suppression effect of different K_{p1}. (a) Overall dynamic waveform. (b) Reducing K_{p1}. (c) Increasing K_{p1}.

C. Verification of NPP balance effect

Fig. 6 shows the NPP balance control effect under different control methods. Fig. 6 (a) adopts the I-D-Σ method proposed in this paper, while Fig. 6 (b) adopts the D-D-Σ method with zero-sequence injection. Similarly, the experimental process in Fig. 6 did not consider the influence of low-frequency CMV. During the testing process, by changing the reference value of the NPP difference, it can be seen that the two methods have the same control effect. However, when the NPP fluctuates, it can cause spikes in the CMV. It has also been proven that the low-frequency CMV is related to the components of NPP balance control. The NPP imbalance will increase the amplitude of the low-frequency CMV.

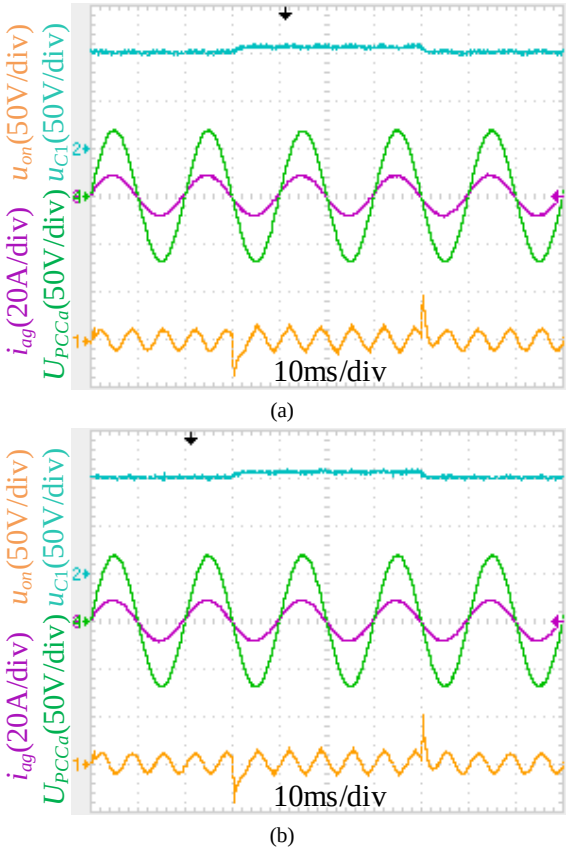

Fig.6 NPP balance control effect of different control method. (a) The proposed I-D-Σ method. (b) The D-D-Σ method with zero-sequence injection.

D. Verification of low-frequency CMV suppression effect

This paper uses FC-CNN to train and predict the collected data of low-frequency CMV. The predicted low-frequency CMV is shown in Fig. 7, with a training set of 8000, a validation set of 2000, and a test set of 4000. From Fig. 7, it can be seen that the learning mechanism of FC-CNN can achieve accurate prediction of low-frequency CMV. Furthermore, the predicted low-frequency CMV is introduced into the control chip to form a lookup table method for injecting low-frequency CMV. Under unchanged operating conditions, low-frequency CMV can be cyclically injected.

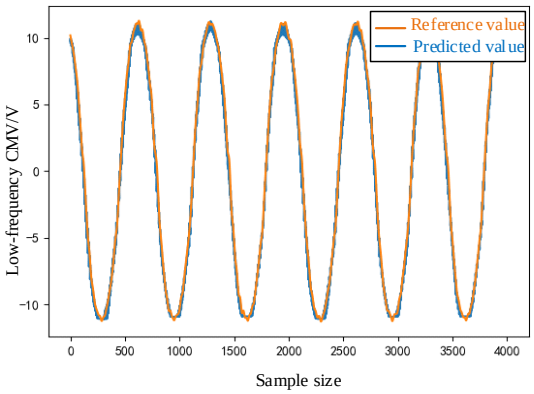

Fig. 7 Waveform of low-frequency CMV estimation results based on FC-CNN.

Fig. 8 shows the comparison waveforms before and after using the I-D-Σ method considering low-frequency CMV. From the figures, it can be seen that the proposed low-frequency CMV estimation method can accurately estimate the CMV, which is achieved through the DA conversion function of the controller. Through comparative experiments, it can be proven that the I-D-Σ method proposed in this paper can effectively reduce the low-frequency CMV caused by the presence of low-frequency components in the modulated wave.

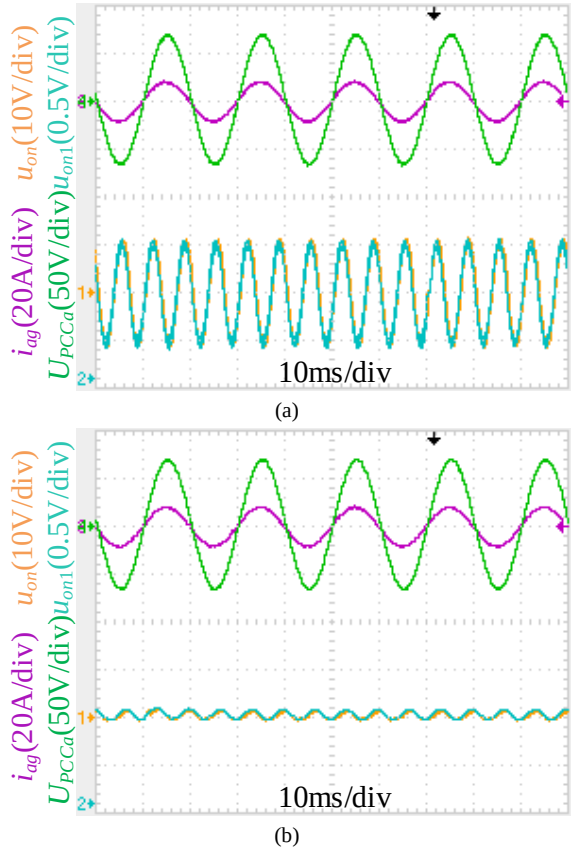

Fig.8 Comparison waveforms before and after using I-D-Σ method considering low-frequency CMV. (a) Without considering low-frequency CMV. (b) With considering low-frequency CMV.

Due to the same derivation process, the effect of grid-connected current tracking and resonance suppression of I-D-Σ method and D-D-Σ method should be consistent under strong and weak grid. This is also demonstrated by the dynamic waveforms under the control parameter changes in Fig. 4 and Fig. 5. The comparative experiment in Fig. 6 can prove that the I-D-Σ method and the D-D-Σ method combined with the zero-sequence injection have the same NPP balancing ability. It has also been proven that the low-frequency CMV is related to the components of NPP balance control. The NPP imbalance will increase the amplitude of the low-frequency CMV. This is because the output voltages of inverter will fluctuate when NPP is unbalanced. The proposed method is similar to the NPP control of the triple fundamental frequency zero-sequence component injection, which will lead to the fluctuation of the low-frequency CMV. In addition, the comparative experiment in Fig. 8 proves that the low-frequency CMV is also suppressed under the condition of equivalent control effect of NPP balance. The I-D-Σ method proposed in this paper has stronger integrated characteristics, and considers grid-current tracking, resonance suppression, NPP balance and low-frequency CMV.

V. Conclusions

In order to solve the problem of multiple and separate control objectives for LCL three-phase T-type three-level grid connected inverters, an I-D-Σ control method based on the D-D-Σ algorithm to achieve integrated multi-objectives control is proposed in this paper. For superimposing the NPP control effect in the D-D-Σ method, a virtual zero potential point is set at the neutral point of DC-side. This method is similar to superimposing the zero-sequence injection component in the modulated wave, and the control effect is also equivalent. Meanwhile, a FC-CNN based low-frequency CMV estimation method is proposed. The estimated result is compensated into the I-D-Σ method, which effectively reduces the amplitude of the low-frequency CMV. The experimental results also verify the effectiveness of the I-D-Σ method proposed in this paper, which realize the integrated control of multi-objectives. Due to the difficulty of estimating high-frequency components, further reduction of high-frequency CMV can be considered by improving the modulation strategy in the future.

References

[1] M. Laaziz, F. Nicolau, M. Ghanes, J. -P. Barbot, R. Boisliveau and N. Machkour, “Fault Detection, Isolation, and Estimation for a Three-Phase Grid Connected DC-AC Inverter with LCL Filters,” *IEEE Control Systems Letters*, vol. 8, pp. 1769-1774, 2024.

[2] A. M. Dos Santos Alonso, L. De Oro Arenas, J. P. Bonaldo, J. De A. olímpio Filho, F. P. Marafão and H. K. M. Paredes, “Power Quality Improvement in Commercial and Industrial Sites: An Integrated Approach Mitigating Power Oscillations,” *IEEE Access*, vol. 12, pp. 50872-50884, 2024.

[3] Z. Hu, X. Xing, C. Liu, R. Zhang and F. Blaabjerg, “A Modified Discontinuous PWM Method for Three-Level Inverters with the Improved LCL Filter,” *IEEE Transactions on Power Electronics*, vol. 39, no. 5, pp. 5498-5509, May 2024.

[4] Y. Han, H. Chen, Z. Li, P. Yang, L. Xu and J. M. Guerrero, “Stability Analysis for the Grid-Connected Single-Phase Asymmetrical Cascaded Multilevel Inverter With SRF-PI Current Control Under Weak Grid Conditions,” *IEEE Transactions on Power Electronics*, vol. 34, no. 3, pp. 2052-2069, March 2019.

[5] A. A. Nazib, D. G. Holmes and B. P. McGrath, "Self-Synchronizing Stationary Frame Inverter-Current-Feedback Control for LCL Grid-Connected Inverters," *IEEE Journal of Emerging and Selected Topics in Power Electronics*, vol. 10, no. 2, pp. 1434-1446, April 2022.

[6] J. S. Costa, A. Lunardi, L. F. N. Lourenço and A. J. S. Filho, "Robust Predictive Repetitive Current Control for a Grid-Connected Inverter Under Parametric Uncertainty," *IEEE Journal of Emerging and Selected Topics in Power Electronics*, vol. 11, no. 5, pp. 4693-4703, Oct. 2023.

[7] S. Ramaiah, L. N and M. K. Mishra, "Loss Modulated Deadbeat Control for Grid Connected Inverter System," *IEEE Journal of Emerging and Selected Topics in Power Electronics*, vol. 11, no. 4, pp. 3715-3725, Aug. 2023.

[8] B. Ren, X. Sun, M. Yu, J. Liu and Q. Zhang, "Circulating Current Analysis and the Improved D–Σ Digital Control Strategy for Multiparalleled Three-Level T-Type Grid-Connected Inverters," *IEEE Transactions on Industrial Electronics*, vol. 67, no. 4, pp. 2810-2821, April 2020.

[9] J. Liu, X. Sun, B. Ren, W. Song and P. Wheeler, "Strong Adaptability Control Based on Dual-Division-Summation Current Control for an LCL-Type Grid-Connected Inverter," *IEEE Transactions on Power Electronics*, vol. 37, no. 12, pp. 14157-14172, Dec. 2022.

[10] J. Xu and S. Xie, "LCL-resonance damping strategies for grid-connected inverters with LCL filters: a comprehensive review," *Journal of Modern Power Systems and Clean Energy*, vol. 6, no. 2, pp. 292-305, March 2018.

[11] S. Luo, F. Wu and K. Zhao, "Modified Single-Carrier Multilevel SPWM and Online Efficiency Enhancement for Single-Phase Asymmetrical NPC Grid-Connected Inverter," *IEEE Transactions on Industrial Informatics*, vol. 16, no. 5, pp. 3157-3167, May 2020.

[12] A. Zorig, S. Barkat and A. Sangwongwanich, "Neutral Point Voltage Balancing Control Based on Adjusting Application Times of Redundant Vectors for Three-Level NPC Inverter," *IEEE Journal of Emerging and Selected Topics in Power Electronics*, vol. 10, no. 5, pp. 5604-5613, Oct. 2022.

[13] F. Chen, W. Qiao, H. Wang and L. Qu, "A Simple Zero-Sequence Voltage Injection Method for Carrier-Based Pulsewidth Modulation of the Three-Level NPC Inverter," *IEEE Journal of Emerging and Selected Topics in Power Electronics*, vol. 9, no. 4, pp. 4687-4699, Aug. 2021.

[14] L. N. Pham, K. D. Pham, Q. D. Phan and N. -V. Nguyen, "Novel Virtual Vector SVPWM Method to Mitigate Low-Frequency Common Mode Voltage for Four-Level NPC Inverters," *IEEE Access*, vol. 12, pp. 22403-22419, 2024.

[15] C. Qin, C. Zhang, X. Xing, X. Li, A. Chen and G. Zhang, "Simultaneous Common-Mode Voltage Reduction and Neutral-Point Voltage Balance Scheme for the Quasi-Z-Source Three-Level T-Type Inverter," *IEEE Transactions on Industrial Electronics*, vol. 67, no. 3, pp. 1956-1967, March 2020.

[16] X. Li, C. Qin, Z. Chu and J. Fang, "A Novel Modulation Scheme for Simultaneous Common-Mode Voltage Reduction and Neutral-Point Voltage Balance in the Reduced Switch Count Quasi-Z-Source Three-Level Inverter," *IEEE Transactions on Power Electronics*, vol. 38, no. 10, pp. 12035-12047, Oct. 2023.

[17] Y. Wang, Y. Yang, S. Chen, et al., "An Improved Model Predictive Voltage Control with Reduced Computational Burden for T-Type Three-Phase Three-Level Inverters," *IEEE Transactions on Power Electronics*, vol. 39, no. 2, pp. 2115-2127, Feb. 2024.

[18] J. -H. Lee, J. -S. Lee, H. -C. Moon and K. -B. Lee, "An Improved Finite-Set Model Predictive Control Based on Discrete Space Vector Modulation Methods for Grid-Connected Three-Level Voltage Source Inverter," *IEEE Journal of Emerging and Selected Topics in Power Electronics*, vol. 6, no. 4, pp. 1744-1760, Dec. 2018.

[19] T. Fang, X. Zhang, C. Huang, W. He, L. Shen and X. Ruan, "Control Scheme to Achieve Multiple Objectives and Superior Reliability for Input-Series-Output-Parallel LCL-Type Grid-Connected Inverter System," *IEEE Transactions on Industrial Electronics*, vol. 67, no. 1, pp. 214-224, Jan. 2020.

[20] Z. Zhou, G. Zhou, Y. Wang, H. Du, J. -S. Hu and C. Yin, "PTV Longitudinal-Lateral State Estimation Considering Unknown Control Inputs and Uncertain Model Parameters," *IEEE Transactions on Vehicular Technology*, vol. 70, no. 5, pp. 4366-4376, May 2021.

[21] H. Sun, R. Madonski, S. Li, Y. Zhang and W. Xue, "Composite Control Design for Systems with Uncertainties and Noise Using Combined Extended State Observer and Kalman Filter," *IEEE Transactions on Industrial Electronics*, vol. 69, no. 4, pp. 4119-4128, April 2022.

[22] S. Sun, T. Wang, H. Yang and F. Chu, "Adversarial Representation Learning for Intelligent Condition Monitoring of Complex Machinery," *IEEE Transactions on Industrial Electronics*, vol. 70, no. 5, pp. 5255-5265, May 2023.

[23] D. Dan, Y. Ying and L. Ge, "Digital Twin System of Bridges Group Based on Machine Vision Fusion Monitoring of Bridge Traffic Load," *IEEE Transactions on Intelligent Transportation Systems*, vol. 23, no. 11, pp. 22190-22205, Nov. 2022.

[24] Z. -H. Liu, X. -H. Li, L. -H. Wu, S. -W. Zhou and K. Liu, "GPU-Accelerated Parallel Coevolutionary Algorithm for Parameters Identification and Temperature Monitoring in Permanent Magnet Synchronous Machines," *IEEE Transactions on Industrial Informatics*, vol. 11, no. 5, pp. 1220-1230, Oct. 2015.

[25] X. Zhang, Y. Hu, C. Gong, J. Deng and G. Wang, "Artificial Intelligence Technique-Based EV Powertrain Condition Monitoring and Fault Diagnosis: A Review," *IEEE Sensors Journal*, vol. 23, no. 15, pp. 16481-16500, Aug. 2023.

[26] C. Gan, W. -H. Cao, K. -Z. Liu and M. Wu, "Dynamic Optimization-Based Intelligent Control System for Drilling Rate of Penetration (ROP): Simulation and Industrial Application," *IEEE Transactions on Industrial Informatics*, vol. 20, no. 3, pp. 3695-3702, March 2024.

[27] H. Li, J. Fu and T. Chai, "Hybrid Intelligent Dynamic Optimization of Switched Systems," *IEEE Transactions on Artificial Intelligence*, vol. 4, no. 6, pp. 1679-1690, Dec. 2023.

[28] K. Wang, J. Chen, Z. Song, Y. Wang and C. Yang, "Deep Neural Network-Embedded Stochastic Nonlinear State-Space Models and Their Applications to Process Monitoring," *IEEE Transactions on Neural Networks and Learning Systems*, vol. 33, no. 12, pp. 7682-7694, Dec. 2022.

[29] K. Duffy, T. J. Vandal, W. Wang, R. R. Nemani and A. R. Ganguly, "A Framework for Deep Learning Emulation of Numerical Models with a Case Study in Satellite Remote Sensing," *IEEE Transactions on Neural Networks and Learning Systems*, vol. 34, no. 7, pp. 3345-3356, July 2023.

[30] N. Ahmad, Y. Ghadi, M. Adnan and M. Ali, "Load Forecasting Techniques for Power System: Research Challenges and Survey," *IEEE Access*, vol. 10, pp. 71054-71090, 2022.

[31] J. Kim and H. -S. Lim, "Neural Network with Binary Cross Entropy for Antenna Selection in Massive MIMO Systems: Convolutional Neural Network Versus Fully Connected Network," *IEEE Access*, vol. 11, pp. 111410-111421, 2023.

[32] M. Fetanat, M. Stevens, P. Jain, C. Hayward, E. Meijering and N. H. Lovell, "Fully Elman Neural Network: A Novel Deep Recurrent Neural Network Optimized by an Improved Harris Hawks Algorithm for Classification of Pulmonary Arterial Wedge Pressure," *IEEE Transactions on Biomedical Engineering*, vol. 69, no. 5, pp. 1733-1744, May 2022.

[33] Y. Maeda, K. Tanimoto, K. Sasayama and H. Takao, "Neural-Network-Based Tactile Perception System Using Ultrahigh-Resolution Tactile Sensor," *IEEE Transactions on Haptics*, vol. 16, no. 4, pp. 504-510, Oct.-Dec. 2023.